Magnitude and Frequency relations: are there geological constraints to the rockfall size?

Corominas, Jordi[1]; Mavrouli, Olga[2]; Ruiz-Carulla, Roger[1]

[1]Division of Geotechnical Engineering and Geosciences, Department of Civil and Environmental Engineering. Universitat Politècnica de Catalunya, BarcelonaTech, Spain.

[2]University of Twente, The Netherlands

Email: jordi.corominas@upc.edu

Abstract. There exists a transition between rockfalls, large rock mass failures and rock avalanches. The magnitude and frequency relations (M/F) of the slope failure are increasingly used to assess the hazard level. The management of the rockfall risk requires the knowledge of the frequency of the events but also defining the worst case scenario, which is the one associated to the maximum expected (credible) rockfall event.

The analysis of the volume distribution of the historical rockfall events in the slopes of the Solà d'Andorra during the last 50 years, shows that they can be fitted to a power law. We argue that the extrapolation of the F-M relations far beyond the historical data is not appropriate in this case. Neither geomorphological evidences of past events nor the size of the potentially unstable rock masses identified in the slope support the occurrence of the large rockfall/rock avalanche volumes predicted by the power law. We have observed that the stability of the slope at the Solà is controlled by the presence of two sets of unfavorably dipping joints (F3, F5) that act as basal sliding planes of the detachable rock masses. The area of the basal sliding planes outcropping at the rockfall scars were measured with a Terrestrial Laser Scanner. The distribution of the areas of the basal planes may be also fitted to a power law that shows a truncation for values bigger than 50 m^2 and a maximum exposed surface of 200 m^2. The analysis of the geological structure of the rock mass at the Solà d'Andorra make us conclude that the size of the failures is controlled by the fracture pattern and that the maximum size of the failure is constrained. Two sets of steeply dipping faults (F1 and F7) interrupt the other joint sets and prevent the formation of continuous failure surfaces (F3 and F5). We conclude that due to the structural control, large slope failures in Andorra are not randomly distributed thus confirming the findings in other mountain ranges.

1. Introduction

Rockfalls are widespread phenomena in mountain ranges, coastal cliffs, volcanos, river banks, and slope cuts. Most of them take place in remote places, but they may cause significant damage in residential areas and transport corridors (Hungr et al. 1999; Chau et al. 2003; Corominas et al. 2005). They are extremely rapid processes that even in the case of small events, they exhibit high kinetic energies and damaging capability (Turner and Jayaprakash, 2012).

Cruden and Varnes (1996) defined rockfall as the detachment of a rock from a steep slope along a surface on which little or no shear displacement takes place. The detached mass experiences free fall and, after impacting on the ground, it continues by bouncing and rolling. Strictly speaking, rockfalls are individual blocks or relatively small rock masses that propagate without interaction between the most mobile fragments (Hungr el al. 2014). Rock avalanche is a large rock mass volume that propagates as granular flow, involving crushing and pulverisation of the particles (Scheidegger, 1973; Hungr et al. 2014).

Rochet (1987) distinguished: (i) falls of boulders up to few hundred of cubic meters, in which no interaction exists between the rock fragments, which follow independent trajectories; (ii) rock mass fall up to few hundreds of thousands of cubic meters in which the interaction between particles is weak as they follow independent trajectories or soon they become independent. This sort of propagation is known as fragmental rockfall (Evans and Hungr, 1993); (iii) very large rock mass fall ($>10^5$- 10^6 m^3) showing strong interaction of particles within the moving mass with the development of internal pressures (possible fluidification) and low energy dissipation; and (iv) mass propagation ($> 10^6$ m^3) that progresses mostly by a translational displacement. Differentiating between all these mechanisms is relevant because rockfalls and fragmental rockfalls are modelled as ballistic trajectories while rock avalanches are simulated as granular flows (Bourrier et al. 2013). The passage from a falling of independent particles to a granular flow is gradual and both mechanisms can coexist in some events. The transition may take place at volumes as small as $5x10^4 m^3$ (Davis and McSaveney, 2002) although other authors raise it up to $10^7 m^3$ (Hsü, 1978). The current practice shows that the agreement in using terms such as rockfall, rockslide and rock avalanche has not yet been reached (Hungr et al. 1999; Chau et al. 2003; Dussauge-Peisser et al. 2002; Guzzetti et al. 2003; Hewitt et al. 2008). In light of these considerations, in this paper we will not consider any volumetric threshold between rockfall and rock avalanches, as recommended by Turner and Jayaprakash (2012).

The management of the rockfall hazard may be based on the Quantitative Risk Analysis (QRA). The QRA is a formal and structured framework that considers the probability and consequences for all the credible hazard scenarios (Ho, 2004; Fell et al. 2008). The management of the rockfall risk is a challenging task. There is a demand for assessing not only the hazard and socio-economic impact in the short term but also for evaluating the consequences of large often unrecorded events. The UN/ISDR (2004) introduced the concept of living with risk in order to develop strategies and undertake actions oriented to the prevention and mitigation of the consequences in developed areas. Living with risk requires the analysis of the potentially hazardous scenarios (Brundl et al. 2009) and in particular, the scenario associated to the Maximum Credible Event (MCE).

The magnitude of landslide is expressed by either the area or volume (Corominas et al. 2014). The former is widely used for landslides because they can be readily measured from maps, aerial photographs or satellite images. The rockfall magnitude is usually expressed as the volume. Risk assessment requires considering the probability or the frequency of different magnitude scenarios for landslides (Picarelli et al. 2005; Rossi et al. 2010; Lari et al. 2014) and rockfalls (Hungr et al. 1999; Agliardi et al. 2009; Wang et al. 2014). The frequency may be expressed as a simple cumulative or non-cumulative manner (Guzzetti et el 2002) or as a frequency density (i.e. number of landslides of a given size divided by the size of the bin) (Guzzetti et al. 2003, Malamud et al. 2004).

Landslides occurring in a specific study site may be characterized by magnitude-frequency relations derived from the empirical data. These relations can be prepared using different approaches and data sources (Picarelli et el 2005): landslide of different ages mapped at one time from aerial photographs and field surveys (Guzzetti et al. 2002; Malamud et al. 2004); landslides for a defined time interval (i.e. from successive aerial photographs); from triggering events such as rain storms or earthquakes (Malamud et al. 2004); from continuous inventories (Hungr et al. 1999; Guzzetti et la. 2003; Rossi et al 2010). The M-F relations often follow a power law over a limited scale range, with deviations at both high and low magnitudes (Brardinoni and Church, 2004; Guthrie and Evans, 2004). To explain the positive exponent at smaller volumes, Stark and Hovius (2001) proposed a double Pareto distribution while Malamud et al (2004) fitted an inverse-gamma distribution but in both cases the tail of the distribution follows a power law.

A scale invariance of the M/F relation has been observed over several orders of magnitudes in landslides and rockfalls, in different geological contexts and associated to different triggering events (Guzzetti et al. 2003; Marques, 2008). Malamud et al. (2004) noted that rockfalls show a frequency-size distribution

different than the other types of landslides. This was attributed to the fact that rockfall involves the disintegration of the rock mass. Guzzetti et al. (2003), Dussauge et al. (2003), and Hergarten (2012) claimed that the negative exponent of the power law is similar for several rockfalls inventories. A wider review of the available literature indicates however that the scaling parameters of the power law for rockfalls may vary between 0.4 and 0.9 according to regional differences in structural geology, morphology, hydrology and climate (Barlow et al. 2012) (see also Table **1**).

Table 1. Exponents of the power law fitted distributions obtained for different rockfall inventories

Reference	Location	Length of the record (yr)	Range of volumes fitted (m^3)	number of events N	Scaling parameter b
Hungr et al. 1999	Highway 99 British Columbia,	40	10^1 to $8x10^8$	390	- 0.43
	BCR line	12	10^0 to 10^4	403	-0.4
	Highway 1		10^0 to 10^4	226	-0.7
	CP Line	22	10^0 to 10^4	918	-0.65
Gardner 1970[a]	Lake Louis	Two summers	10^{-1} to 10^3	409	-0.72
Chau et al. 2003	Hong Kong, China			201	-0.87
Dussauge-Peisser et al 2002	Upper Arly, gorge French Alps		10^0 to 10^4	59	-0.45
	Grenoble, French Alps	60	10^{-2} to 10^6	87	-0.41
	Yosemite, USA	77	10^0 to 10^5	101	-0.46
Royán et al. 2015	Puigcercós, Spain	6.87	10^{-2} to 10^2	3096	-0.72
Wang et al. 2014	Feifeng Mountain, China	200	10^0 to 10^2	27	-0.62

[a] Cited in Hungr et al 1999

The fact that different sets of rock falls and rock slides exhibit the same magnitude-frequency relation has supported the idea that the frequency of large unrecorded events can be estimated by extrapolating the power law obtained for the small-size events provided that the record of the latter is complete (Dussage-Peisser et al. 2002; Guzzetti el al., 2002, 2003; Picarelli 2005). This exercise raises the question on the range of validity of the extrapolation (Corominas and Moya, 2008). The analysis of the probability of occurrence of rockfalls along large cliffs is affected by uncertainties due to the different site-specific characteristics (Wang et al 2014), while the temporal resolution over which power laws can be applied is poorly constrained (Cruden and Hu, 1993).

The question posed here is to what extent the empirically-based models are capable to extrapolate short-term observations to the spatial and temporal scales required for reliable rockfall risk management. This requires the understanding of the scaling behaviour of rockfall processes. Two issues must be addressed. The first one is that several authors (Picarelli et al 2005; Cascini et al. 2005; Corominas and Moya 2008) argue that a major difficulty for the assumption of M/F invariance is whether the rate of landslide occurrence will persist in the future. In that respect, Cruden and Hu (1993) noticed a decay in time of the number of large landslides in the Canadian Rockies, that contradicts the stationarity implicit in the power law. The second one is the definition of the largest volume that can be predicted with the extrapolation of the M/F relations.

In this paper we attempt to address the last issue with the analysis of the rockfall activity in the Sola d'Andorra, Eastern Pyrenees. We will first present the results of the F/M of rockfalls in Andorra using historical data. Secondly, we will address the definition of a cut-off value for the size of the maximum expected rockfall/rock avalanche event, and we will discuss the role of the geological factors in possible constraining the maximum volumes.

2. Rockfall hazard management in Andorra

The slopes of the Solà d'Andorra bound the right bank of the Valira d'Orient river in the Principality of Andorra. This stretch of the valley is a basin that was deepened and widened by glaciers during the Pleistocene. After the glacier retreat, a lake was formed and the basin filled with lacustrine, deltaic and colluvial sediments up to a thickness of 100m. Nowadays it forms a 1km-wide alluvial valley (Turu et al. 2007).

The Solà is the lower part of the Enclar massif (2383m), extending between the urban settlements of Santa Coloma and Andorra la Vella. The rock mass is made up of highly fractured granodiorite and hornfels. The slope is characterized by the presence of V-shaped couloirs alternating with steep walls for a length of about 3km (Figure **1**). The couloirs extend from 990 m to about 1300 m.a.s.l. The rockfall activity at the Santa Coloma is associated to the granodiorite outcrops (about 2 km length) and has an average frequency of 1 event bigger than $1m^3$ every 2 years. In the last decades (since the 1960s) the maximum recorded rockfall events attained a volume of 1000 m^3 in the Tartera de la Pica (April 1969) and 150 m^3 (April, 2008) in the chute of Forat Negre. The average annual rainfall precipitation is of 1071.9 mm. Although some events occurred after rainfall episodes, a direct relation between

precipitation and rockfalls could not be established so far (Copons et al. 2004). Freeze-thaw process might also play a role for the onset of the failure.

Figure 1. The slope above the town of Santa Coloma and the chute of Forat Negre.

The efforts of the Andorran administration in the management of natural hazards began in the eighties of last century (Corominas, 2007). The first global initiative took place between 1989 and 1991 with the preparation of hazards maps at 1:25,000 scale, that included landslides and flood-prone areas. The main impulse in management of the natural hazards was given by the Urban and Land-Use Planning Law approved in 1998. The key points of this law in terms of hazard management are the following (Escalé, 2001): (a) the zones exposed to natural hazard cannot be developed; (b) local development plans must take into account the presence of zones exposed to natural hazards; (c) the Andorra government will commission both geological-geotechnical studies and hazard mapping. This means that the Andorra government has to provide hazard inventories, hazard zoning and regulations for management of the threatened areas. In those sites where hazard can be mitigated and reduced to an acceptable level, the Andorran government will establish the requirements of the protective works that have to be undertaken. After the implementation of the law, several studies were completed and among them: the Geotechnical and Landslide Hazard Zoning Plan of Andorra (1999-2001). The purpose of the Plan was to identify, locate and assess the natural hazards as well as the geological and geotechnical constraints that may

affect future construction works in the Andorran territory. The scale of work was 1:5,000 (Corominas, 2007).

In January 1997, a falling rock block hit a building in Santa Coloma, causing an injury. This event persuaded the Andorran administration to implement the Rockfall Risk Management Master Plan (RFMP) of the Solà d'Andorra which was completed in 1998 (Copons et al. 2004). This Plan established, the restriction to the development in the most threatened sectors and it was published in the official journal of the Principality in the year 2000. The RFMP, based on a rockfall trajectographic analysis, defined an upper boundary line above which development is forbidden. Several existing buildings were already within the exclusion area. For all these cases, the RFMP contemplated the design of rockfall defenses (Copons et al. 2001). The cost of the protective works raised over 4.5 million euro (Escalé, 2001). After the construction of the fences several events have occurred with minor only consequences. However, a residual risk exists as large rockfall events might not be fully retained due to excessive energy or bouncing height (Corominas, et al. 2005).

The RFMP has been complemented with a Surveillance Plan that started in 1998. This Plan aimed at (Amigó et al. 2001): (a) the inventory of the rock falls occurring in the valley side; (b) the update and validation of the trajectographic models used to design the protective structures (rockfall paths, height of bounces, among other parameters); and (c) the detection of possible large rockfall events (exceeding thousands of m^3). It is expected that before the large rock mass failure, premonitory signs such as the increase the number of small rockfall events or the opening of new fractures, could be timely identified.

The risk management practice requires assessing the scenario associated to the maximum credible event (MCE). The MCE is a very conservative estimate of the event considered sufficiently unlikely, sometimes associated to a notional return period of the order of 1,000 years (Ho, 2004). In any case, it should correspond to the largest event observed in historical data, geomorphological evidence in the area and its vicinity and any other relevant evidence from similar terrain (Ho, 2004).

We have attempted to estimate the size of rockfall events that can be expected in the future. A 50-yr length record of rockfall events bigger than 1 m^3 is nowadays available in Andorra and can be considered complete since 1999. This length is similar to the length used in other M/F studies (Hungr et al. 1999; Dussauge-Peisser et al 2002). The record has been used for the construction of the M/F relation for the Solà d'Andorra. Table **2** contains the historical rockfalls inventoried and their volumes, while the plot

of Figure 2 shows the relationship between the volumes and the cumulative frequency expressed as the number of events greater than a given volume per year.

Location	Year of occurrence	source	Volume (m^3)	Largest block (m^3)
Canal de la Pica	1969	Copons, 2007	1000	60
Canal Ramenada	2012	MOT	450	
Canal de la Pica	20003	Copons, 2007	300	70
Forat Negre	2008	MOT	150	32
Canal de l'Alzina	1997	Copons, 2007	125	25
Canal Ramenada	End of 1960s	Copons, 2007	100	10
Roc Sant Vicenç	2002	MOT	30	14
Forat Negre	1968	Copons, 2007	30	7.5
Forat Negre	2009	MOT	30	7
Forat Negre	2004	MOT	25	4
Canal Coll d'Eres	1983	Copons, 2007	25	7
Forat Negre	2014	MOT	20	8
Cementiri	2011	MOT	20	1.3
Forat Negre	1984	Copons, 2007	10	1
Forat Negre	2002	MOT	10	2
Forat Negre	2003	MOT	10	2.3
Canal Boneta	2001	MOT	10	
Canal Boneta	2002	MOT	10	1
Canal de la Pica	1996	Copons, 2007	10	2
Canal de la Pica	2000	MOT	10	
Forat Negre	1994	Copons, 2007	5	
Forat Negre	1996	Copons, 2007	5	
Canal de l'Alzina	1999	Copons, 2007	5	
Forat Negre	2000	MOT	4	
Forat Negre	2001	MOT	4	

Table 2. Historical rockfalls at the Solà d'Andorra and their volumes. The rockfall volumes of the boxes framed in pink are estimations based on the volume of the largest block observed. Source: Copons, 2007 and unpublished data from Surveillance Plan of the Ministry of Land Management (MOT).

The inventory includes 25 cases since the late 60s of last century. The data before 1999 might not be complete and, in some events, the initial rockfall volume is not well known. For this reason, an estimate has been made (boxes highlighted in pink) from the descriptions available of the events.

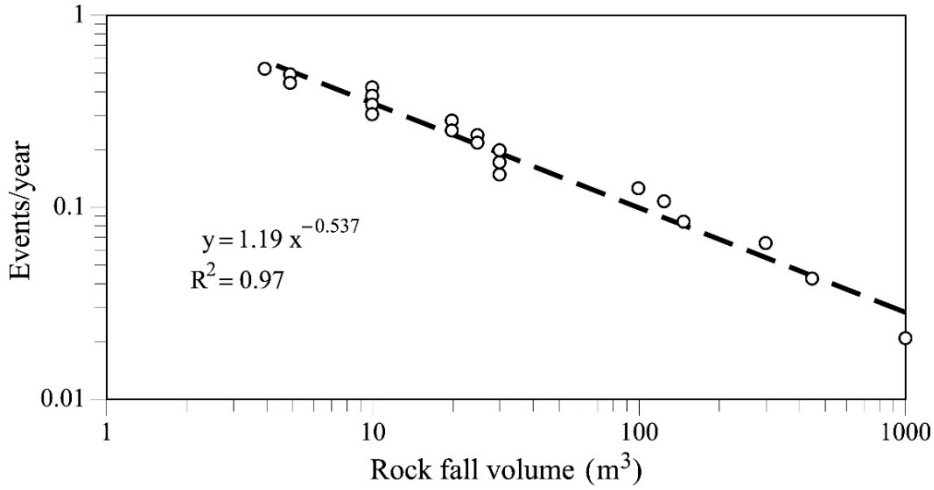

Figure 2. Relationship between the volume (m^3) of the inventoried rockfall event at the Solà and the cumulative relative frequency (N events larger than a certain size per year)

The relation shown in Figure 2 fits well to the power law of Equation [1]:

$$N = 1.193.\ V^{-0.537} \quad [1]$$

Being N, the number of rockfalls per year exceeding the volume V.

The extrapolation of this relationship to rockfall volumes much larger than the inventoried, would result in the frequencies and return periods for each range of volumes shown in Table 3.

Volume range (m^3)	Fr (events/year)	Return period (years)
≥ 1	1.1933	0.84
≥ 10	0.3465	3
≥ 100	0.1006	10
≥ 1,000	0.0292	34
≥ 10,000	0.0085	118
≥ 100,000	0.0025	406

≥ 1,000,000	0.0007	1397

Table 3. Cumulative frequencies and return periods obtained from the extrapolation of the power law fitted to the rockfalls observed at the Solà d'Andorra during the last 50 years.

The extrapolation of the power law defines a scenario in which cliff failures with a magnitude of a hundred of thousands of cubic meters (i.e. large rock slides or rock avalanches) have a recurrence period of about 400 years.

3. Are there evidences supporting the extrapolation of M/F relation obtained at the Sola d'Andorra?

A number of studies have shown that the occurrence of large rockslides and rock avalanches has geomorphic consequences which can be deciphered by means of the analysis of the landscape. Two main distinct features of rock avalanches are the deposits and the scar left at the source (Soeters and Van Westen, 1996; Hewitt, 2002; Ballantyne and Stone, 2004).

3.1 Rockfall deposits

Rock slide and rock avalanche deposits as old as tens of thousands of years remain blanketing the valley bottoms of the main alpine chains (Voight and Pariseau, 1978; Cave and Ballantyne, 2016; Crosta et al. 2016). Some old rock-avalanche deposits are remarkably well preserved such as those of the Karakoram range (Hewitt et al. 2008) or in the northern Chilean coast (Crosta et al. 2016), partly due to semi-arid conditions of these regions. Others are less preserved because they run onto glaciers and became dispersed by ice flow or removed by the fluvial erosion (Hewitt et al. 2008). However, even in the latter case the deposits may remain for thousands of years.

The Valira d'Orient glacier resided in the Andorra la Vella basin until ca. 18 ka (Turu et al. 2016). After the glacier retreat any landslide or rockfall deposit would have emplaced on ice-free valley floor. At present, only talus deposits from rockfalls and the debris cones from debris flow events accumulate at the foot of the slopes, bounding plain of the Valira river. According to the results of Table 2, rockfalls of the order of 10,000 m^3 should have occurred almost every 120 years and two events of 100,000 m^3 each millennium. However, the bottom of the the Solà d'Andorra lacks of debris deposits that could be associated with the release of a large rockfall or rock avalanche. In case they had occurred, the deposits

should lay over the alluvial plain of Santa Coloma. Figure 3 shows the topographic profile of the Santa Coloma slope, the alluvial plain of the Valira river, and the expected runout for different rockfall/rock avalanche sizes detached from the walls of the Solà d'Andorra. The runout has been determined using the equations for unobstructed rockfalls/rock avalanches prepared by Corominas (1996) and Corominas et al. (2003).

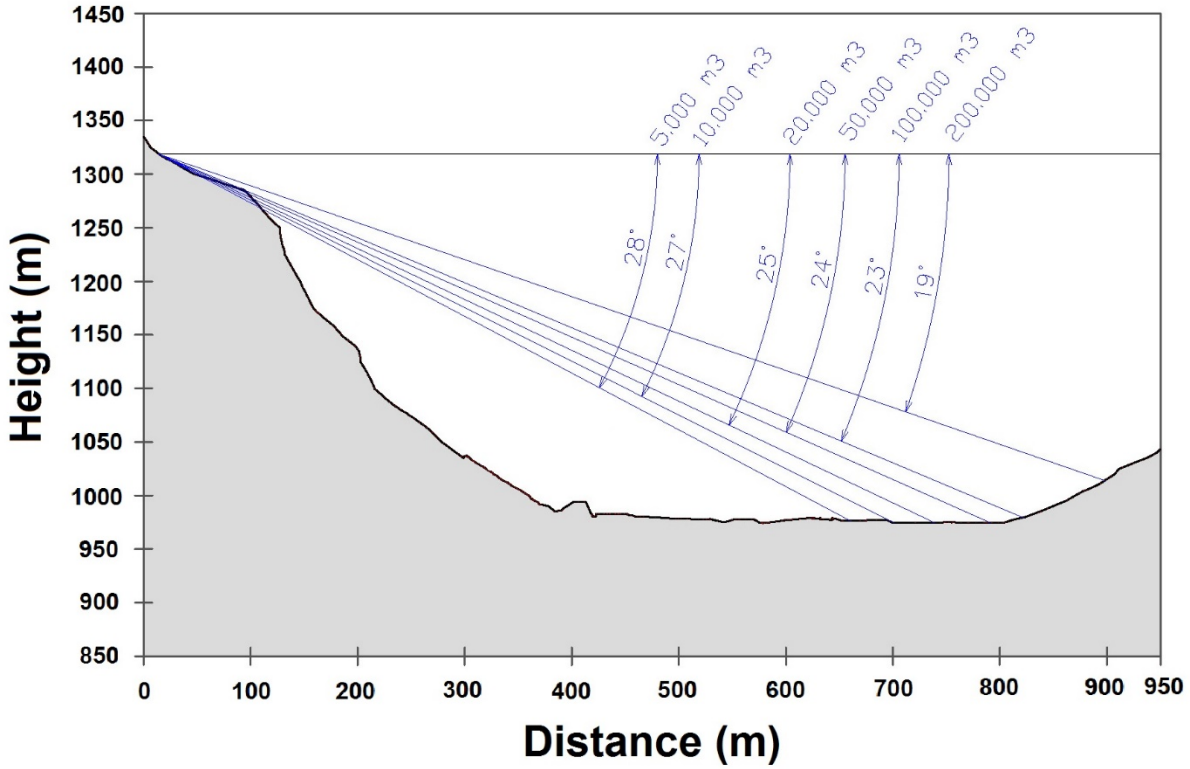

Figure 3. Maximum runout that could be achieved by rockfall events with sizes between 5,000 and 200,000 m^3 originating from the slopes of the Borrassica in Santa Coloma if they had occurred in the past. The runout has been calculated following the criterion of reach angle for unobstructed rockfall events (Corominas 1996; Corominas et al. 2003)

Based on the distances obtained shown in Figure **3**, rockfall events of tens of thousands of cubic meters would blanket much of the valley bottom. In the event that the volume increased to 100,000 m^3 or greater, the deposits would reach the opposite slope. However, in the historical archives of the valley there is no record of events of any of these sizes. Figure **4** is an aerial photograph taken before the extensive development of the basin of Andorra la Vella and Figure **5** is the geomorphological map prepared by Turu et al (2007). Both figures show the lack of rockfall/ avalanche deposits over the valley bottom. These type of deposits have not been found either in the boreholes drilled in the fluvial plane or in the interpretation of geoelectrical surveys carried out in the basin for hydrogeological purposes (Gutiérrez-Rodríguez and Turu, 2013).

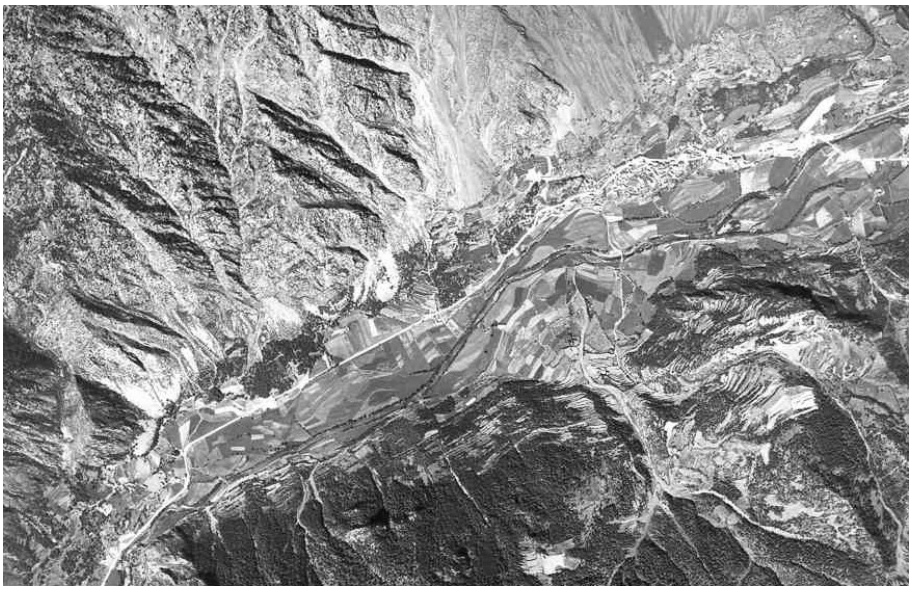

Figure 4. Aerial photograph of the Andorra la Vella basin taken in 1948.

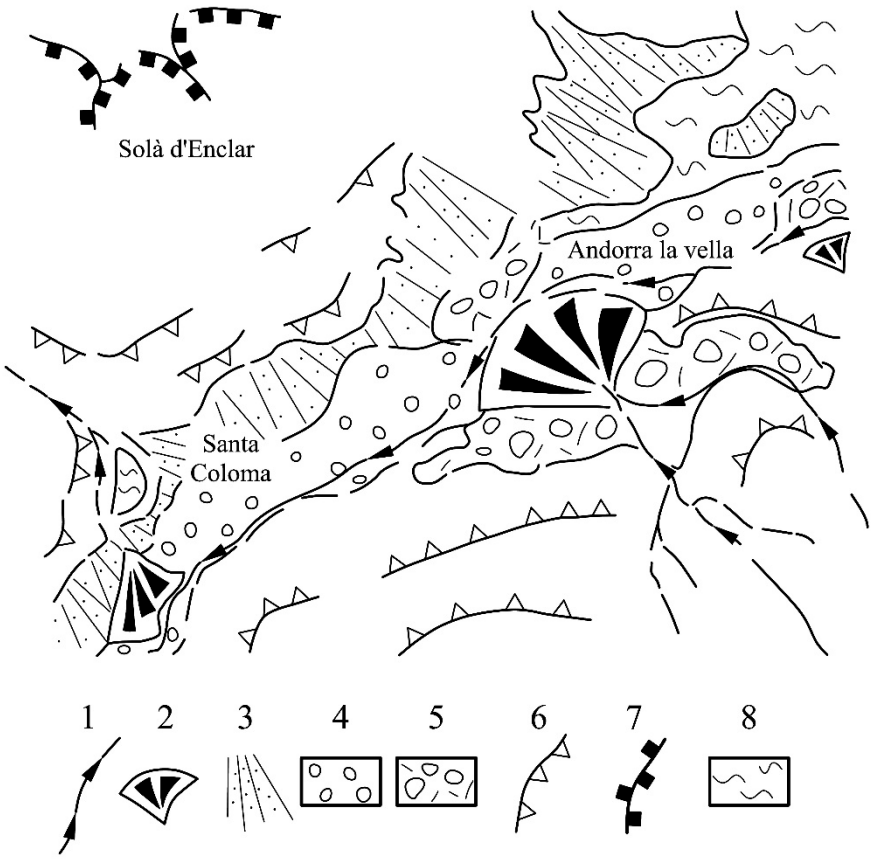

Figure 5. Geomorphological map of Santa Coloma – Andorra la Vella – Les Escaldes: (1) stream, (2) debris fan, (3) talus deposit and colluvium, (4) alluvial deposit, (5) till, (6) reconstructed glacial margins, (7) glacial cirque, (8) hummocks (modified from Turu et al. 2007)

3.2 Analysis of the rockfall scars

The availability of modern data capture techniques facilitates the analysis of the rockfall scars. Successive surveys with the TLS allow the identification and measure of the volumes missing from the rock wall (Rosser et al. 2007) and the preparation of M/F relations (Royan et al. 2014). We argue that cliff faces contain the record of rockfall events that occurred during the last hundreds or thousands of years. Each rockfall scar bounds the mass that was detached from the rock wall as a single or multiple events (Figure **6**). Consequently, the volume distribution of the rockfall scars can be used as a quantitative proxy for the rockfall volume distribution. The scar volume distribution has been determined indirectly using a stochastic simulation based on the distributions of the observed basal areas and the scar heights (Santana et al. 2012).

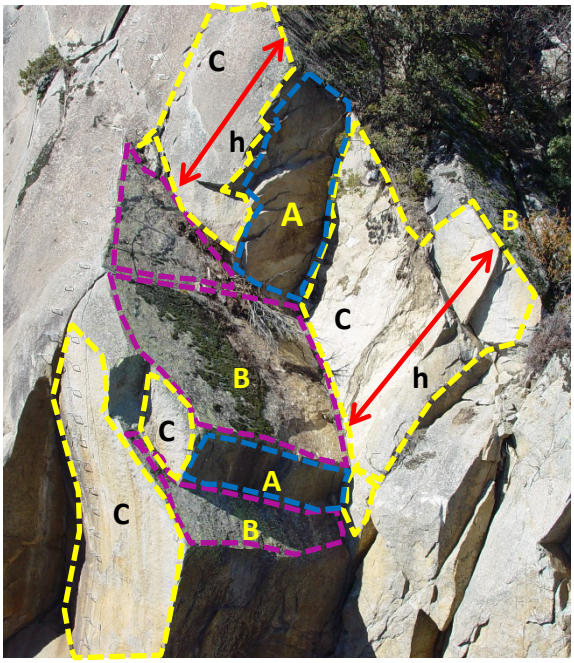

Figure 6. Rockfall scar defined by three intersecting joint sets. The detached block was resting on a basal plane (B) which is bounded by planes (A) and (C). The height of the scar (h) may involve several spacings

The dimensions of the rockfall scars can be determined from a point cloud obtained with a Terrestrial Laser Scanner, TLS. In the the Solà d'Andorra this was carried out at the slope of Borrassica-Forat

Negre, following the methodology of Santana et al. (2012). Eight joint sets present in the rock mass were first identified (F1 to F8). Four sets are directly involved in the formation of the scars (Table **4**).

Table 4. Dip direction and dip angle of the discontinuity sets that contribute to the formation of scars.

	Dip direction (°)	Dip angle (°)	Role
F1	54	59	Lateral plane/tension crack
F3	157	56	Basal sliding plane
F5	182	47	Basal sliding plane
F7	141	89	Tension crack

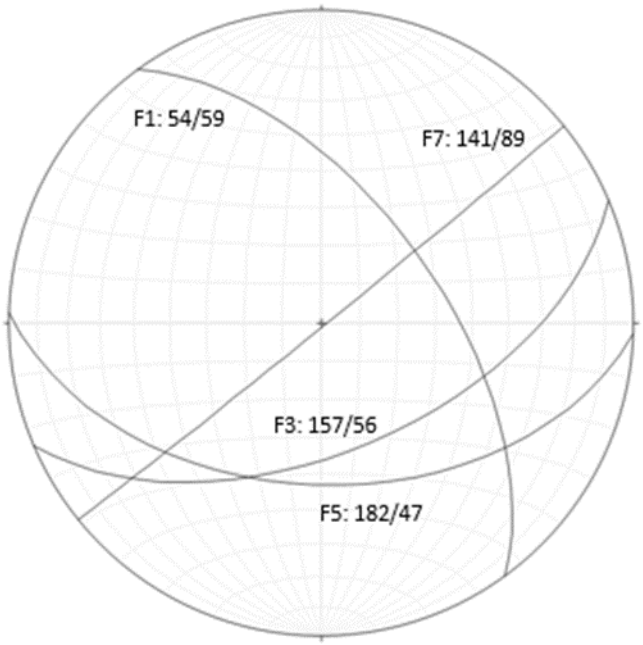

Discontinuity set	Dip direction (°)	Dip angle (°)	Role
F1	54	59	Lateral plane/tension crack
F3	157	56	Basal sliding plane
F5	182	47	Basal sliding plane
F7	141	89	Tension crack

Figure 7. Stereoplot showing the joint sets involved in the formation of unstable volumes at the slope of Borrassica-Forat Negre. The slope is mostly oriented to 180º and has an overall slope angle of 67º

The observation of historical events as well as the kinematic analysis of the fracture pattern (Figure **7**) show that most of the rockfalls initiate by sliding of the detached rock mass over an unfavourable dipping discontinuity plane (F3 and F5). Each rockfall scar is therefore defined by a basal plane and two tension cracks (F1, F7 joint sets). The area of each discontinuity plane and the heights of the scars were obtained from the treatment of the point cloud generated with the TLS. The volume of the simulated rockfalls was generated stochastically by combining the measured areas and the scar heights following a Monte Carlo simulation approach. The procedure accounted for stepped failures sliding over parallel discontinuity surfaces spaced less than 0.2 m. It is assumed that each scar on the slope face corresponds at least to an event.

To simulate the size distribution of the missing volume from the scars, the points of the point cloud belonging to each sets were extracted and planes were adjusted to them. Afterwards, the areas were measured (Figure **8**) as well as their maximum width (along the strike) and length (along the dip direction).

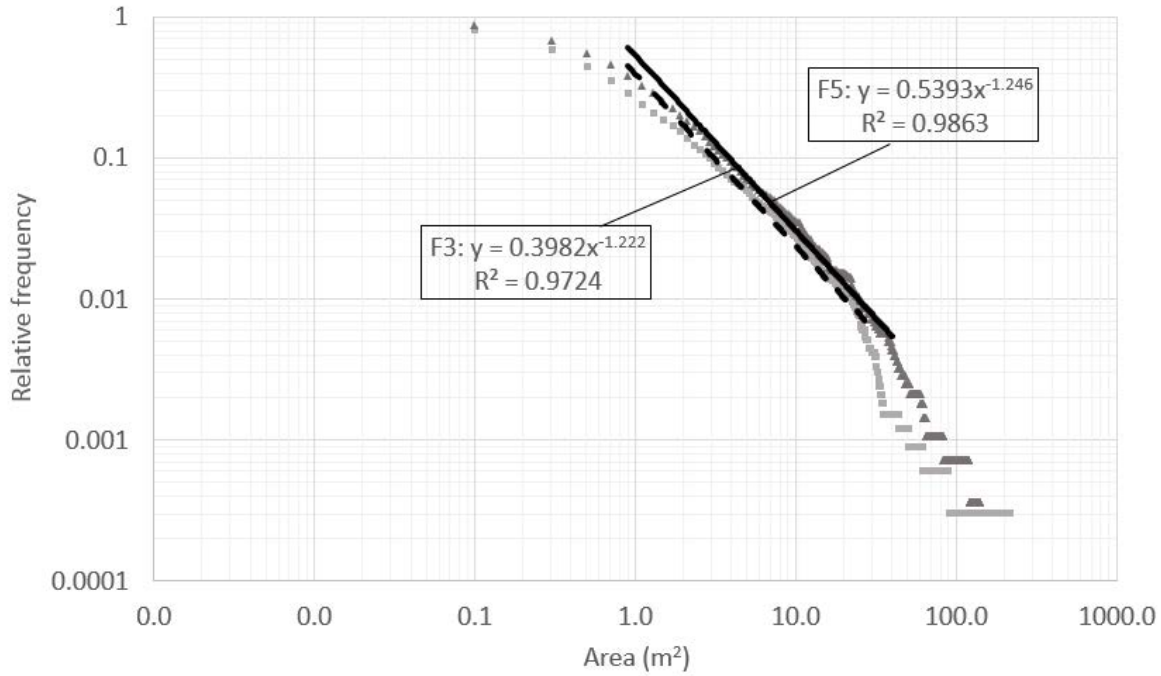

Figure 8. Magnitude (area in m^2) - Cumulative frequency of the discontinuity surfaces of the sets F3 and F5, calculated from the point cloud

The areas of F3 and F5 (basal planes of the scars) were well fitted to a power law. The scar heights were measured as intersections of the tension cracks F1 and F7. Eventually, the size distribution of the scars was calculated past a Monte Carlo simulation by the multiplication of the scar areas with the scar heights (see details in Santana et al. 2012).

The results were fitted to the power law of Equation [2].

$$N (>V) = 1919V^{-0.92} \quad [2]$$

Where N is the number scars bigger than V and V, the volume of the scar in m^3.

Five thousand scars were randomly generated, based on the observed distribution of the areas and heights, which is of the same order of magnitude of the number of scars identified on the point cloud in Borrassica-Forat Negre. The maximum scar volume calculated using this method is about 3000 m^3. This volume is substantially smaller than the predicted with the extrapolation of the M/F relation of the historical rockfalls.

The analysis of large rockslides, show that the sliding surface may be a single plane or it may be composed of a series of sliding planes and lateral release surfaces with both down-dip and laterally stepped morphology as in the Aknes (Ganerod et al. 2008) or Palliser Rockslide (Sturzenegger and Stead, 2012). In the latter case, a composite surface is generated, which is characterized by a combination of low persistence discontinuities, cross joints and broken rock bridges. Steps can be as high as 35m (Sturzenegger and Stead, 2012). The approach followed by Santana et al (2012) in the slopes of Borrassica-Forat Negre has the restriction that only step path basal surfaces involving steps heights of less than 0.2m were considered.

3.3 *Identification of massive rock mass failure scars*

To check the possibility of occurrence of a large stepped failure at the Borrassica-Forat Negre slope in the past, we have looked for remnant of an old rockslide or rock avalanche scar in the slope. Source areas of large rock slides and massive rock failures are usually characterized by the presence of a more

or less continuous sliding surface that terminates against large lateral and or back release surfaces forming prominent scarps (Cruden 1975; 1985; Eberhardt et al 2004; Willenberg et al. 2008; Sturzenegger and Stead, 2012; Stead and Wolter, 2015). Lateral and back release surfaces can form by the presence of cross joints, by the breakage of rock bridges or by the combination of both. In highly unstable mountain fronts, adjacent scars may coalesce to form large niches several kilometres length (Crosta et al. 2016). These features can persist for millennia or even longer (Hewitt et al 2008).

The exposed basal sliding planes (failure surface) are therefore a reasonable indicator of both the occurrence and size of rock slide (rock mass failure).

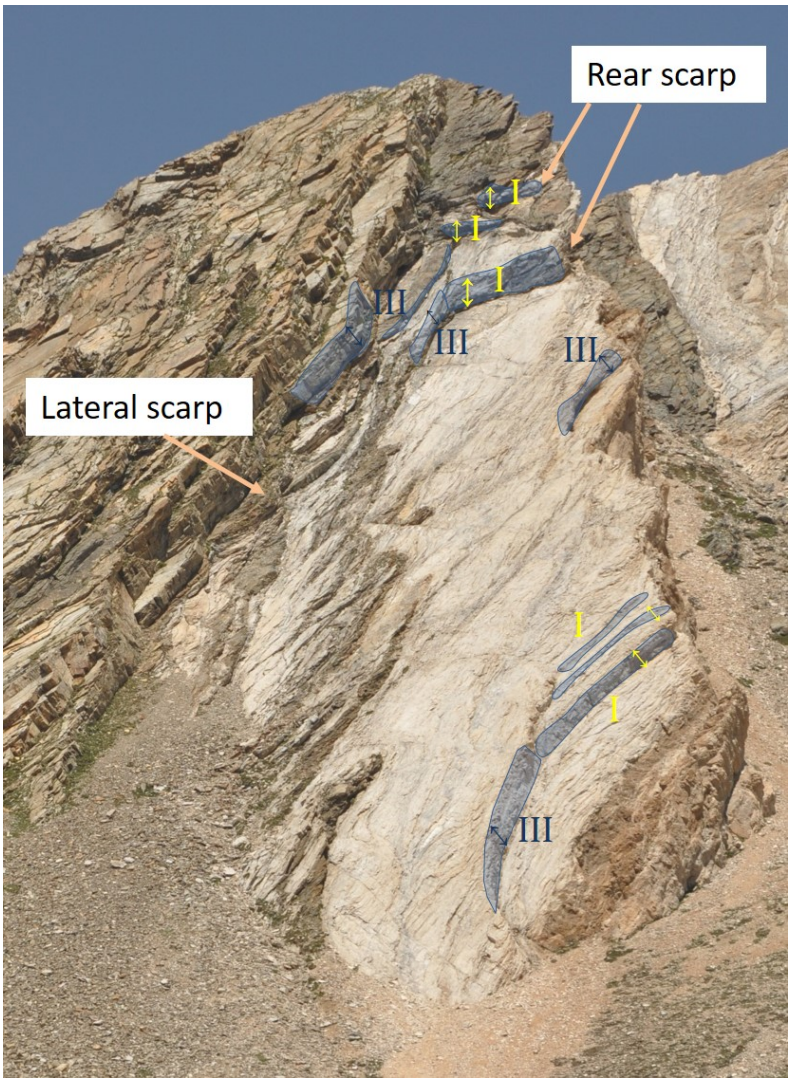

Figure 9. Type I and III steps (Sturzenegger and Stead, 2012) formed at the down-dip and laterally stepped basal failure surface of a rockslide at the Pic of Freser, Eastern Pyrenees, Spain

At the scale of the whole slope, both rear and lateral scarps and either single or step path sliding surface may be identified as a distinct macro forms (*Figure **9***). The steps of the stepped sliding surfaces, can be approximated as roughness features (Wolter et al. 2014; Stead and Wolter, 2015) that can be scaled (Barton and Bandis, 1982).

We have attempted to fit a large step path surface at the slope of the Borrassica-Forat Negre, assuming that the surface can be a down-dip (type I) or a laterally (type II) stepped basal failure surface or both. We expect the large stepped failure to be composed of more or less parallel, relatively long, straight stretches alternating with steps of different heights produced by F7 joint set. The direction of the movement will follow the dip direction of either F3 or F5 joint sets. It may be also expected that lateral steps (type III) may develop in a direction more or less parallel to F1 joint set. In this case, transverse cross sections should show straight (almost horizontal) stretches alternating with the steps generated by F1 joint set, similarly to what is shown in Figure **10**.

We used the program CloudCompare to fit a large rupture surface to a sequence of down-dip stepped planes and to obtain the cross-sections. As seen in Figure **10**, it is not possible to adjust a large stepped surface to Borrassica-Forat Negre slope because despite the longitudinal profile being compatible with the presence of a large stepped surface, the transverse profiles suggest otherwise. The transverse profiles show protuberances that prevent the definition of a sliding surface. We have included the profile generated in the outcrop of Pala de Morrano in the Aigüestortes-Sant Maurici National Park, Central Pyrenees, for comparison.

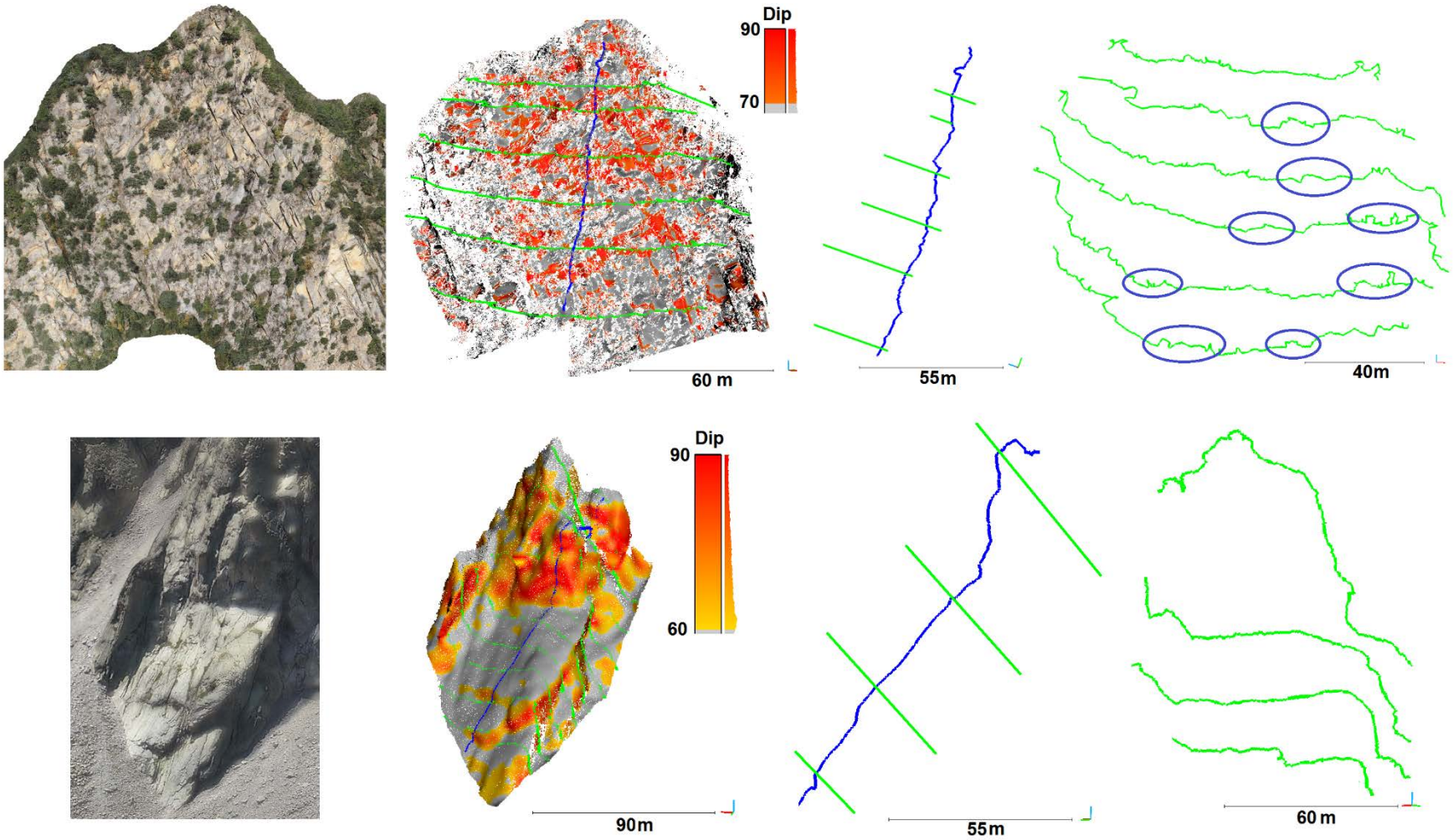

Figure 10. Top: profiles extracted from the point cloud of the slope of Borrassica-Forat Negre. Transverse sections exhibit protuberances that interrupt any possible large sliding surface. Bottom: profiles extracted from a point cloud in Pala de Morrano, Aigüestortes i Estany de Sant Maurici National Park, Eastern Pyrenees. The straight stretches of the step-path failure surface are clearly observable in both longitudinal and transverse cross-sections.

4. Defining the maximum credible volume

In risk management, the design of mitigation measures and the delimitation of the hazardous areas are based on analyses for a range of expected potential rockfall volumes (Corominas et al. 2005; Abruzzese et al. 2009; Agliardi et al. 2009; Li et al. 2009). The question posed in our work is what the range of validity of the historical power law is and specifically, what the largest rock slope failure or maximum credible event (MCE) can be in the Borrassica-Forat Negre slope. The MCE is usually characterized by volumes of rock masses of several orders of magnitude greater than the events commonly observed in the study area.

As already mentioned, power laws for rockfalls-rock avalanches have been verified by a range of volumes spanning several orders of magnitude as in Yosemite, U.S.A. (Guzzetti et al. 2003) but in the case of the Solà d'Andorra, the extrapolation of M/F calculated from the historical rockfalls is not in agreement with the geological (Holocene) record. On the other hand, the maximum volume cannot be unlimited. It is evident that for a given slope, the failure cannot exceed the size of the slope (Guzzetti et al. 2002). In the Solà d'Andorra this would be the scenario of an unfavorably oriented fully persistent discontinuity outcropping at the base of the cliff, crossing the entire massif. However, the largest credible rockfall event is the reasonable largest event, not the largest conceivable event.

The analysis of the MCE for rockfalls is not a standardized procedure. In other scientific disciplines, concepts such as the maximum credible earthquake or the probable maximum flood were already introduced in the 90s. For earthquakes, the maximum credible event is the one that can be justified by all the known geological and seismic data (US Bureau of Reclamation, 2015). The estimation of largest hypothetical earthquake takes into account the characteristics of the fault or other seismic source and the current tectonic setting. It can be evaluated either deterministically or probabilistically. As regards the calculation of annual exceedance probabilities of maximum flood discharge, the use of data from multiple sources is recommended. Moreover, procedures have been proposed to obtain the optimal range for the credible extrapolation of the magnitudes and return periods (Swain et al. 2006). In these cases, an upper boundary for the size of the maximum event is obtained.

We assume in our work that the MCE for rockfalls is the largest reasonably conceivable slope failure that appears possible in the geographically contained slope, under the presently known or presumed geostructural and geomechanical setting. Several factors account for the occurrence of a slope failure of

a given size, reflecting the complex interaction between the rock strength properties, the rock mass structure, the geomorphic context and the triggers.

4.1 MCE based on a simple kinematic analysis (Markland test)

As mentioned, the rockfall events in the Solà d'Andorra are mostly governed by the presence of unfavorably dipping joint sets (the discontinuity sets F3 and F5). The potential of a large slope failure generated by this structural setting has been analyzed by Mavrouli et al (2015) and Mavrouli and Corominas (2017). They carried out an analysis aimed at identifying large kinematically detachable rock masses on a Digital Elevation model, DEM. The potentially unstable volumes were detected by checking the compliance of the joint sets with the Markland criteria at every cell. Adjacent unstable cells on the DEM, were merged to form larger unstable zones (Figure **11**).

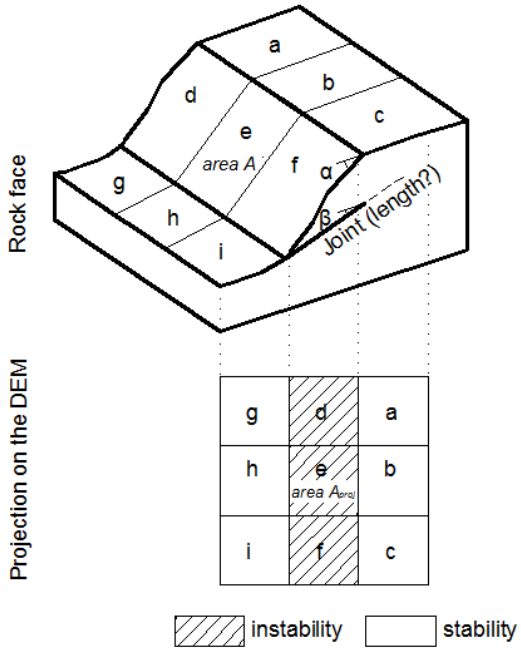

Figure 11. Rock wall and its projection on the mesh of the Digital Elevation Model. It assumes infinite lateral persistence of the unfavourable joint sets. Thus, adjacent cells which meet the requirements of the Markland test merge to form a single kinematically movable rock mass. (from Mavrouli et al. 2015)

The volume of the detachable masses was calculated from the kinematically unstable slope area assuming either cubic or prismatic shape. A power relation between the area and the volume is used, similar to the empirical relations found in the literature (Guzzetti et al. 2009, Klar et al. 2011). The distribution of the potential rockfall volumes was calculated. The largest volumes obtained are of the

order of 50,000 and 25,000 m^3 for cubic and prismatic volumes respectively. The largest basal area was estimated at 1,361 m^2.

The results may be fitted to the power laws of Equations [3] and [4].

$$N(>V) = 817.74V^{-0.572} \quad [3]$$

$$N(>V) = 952.42V^{-0.546} \quad [4]$$

For cubic and prismatic shapes, respectively and volumes V>100 m^3

Where N is the number of scars bigger than V and V, the volume of the scar in m^3.

4.2 MCE based on discrete potentially movable volumes

We have here approached the assessment of the MCE using an alternative way. In this procedure, we identified and calculated the volume of real rock spurs resting on unfavourable dipping basal planes (F3 / F5 sets) of the Borrassica-Forat Negre slope, with several unconstrained faces. The basal sliding surfaces are actual outcropping discontinuities that have been identified one by one. The surfaces have been extracted from the TLS-generated point cloud and confirmed with digital photos. A similar approach was used by Gigli et al. 2014.

The calculation of the volumes has been made with the program Rhinoceros. We have followed these steps:

1) Identification of rock spurs having at least three unconstrained slope faces (front, upper, and lateral), permitting mobilization.
2) Location of both the basal and lateral discontinuity planes that bound the rock spur and definition of the volume of the rock mass.
3) Estimation of the volume of the rock mass formed by the intersection of these discontinuity planes with the surface topography.

An example of the procedure followed is shown in the Figure **12** (A to C).

Figure 12. (A) Identification and definition of the rock spur volumes kinematically detachable at the Borrassica and Forat Negre slope. Each volume is delimited by real discontinuity planes observed in the slope and at least,

three unconstrained faces; (B) Extraction of the of rock mass volume defined at (A). The in the back (brown), is just an auxiliary plane used to bound the mass and calculate the volume; and (C) Representation and calculation of the volume of rock mass defined at (A). In this case, the calculated volume is 9900 m^3

Following this procedure, we have characterized the five largest rock volumes of the Borrassica slope resting on a basal plane, matching with the orientations of F3 or F5 joint sets whose outcrops have been double-checked in the photographs (Figure **13**). These volumes are bounded by the topographic surface only except the one of 7400m^3 which is interrupted by the highly persistent F1 and F7 joint sets, that form high scarps around the detachable mass. In the latter case it is assumed that the basal plane maintains its continuity under the rock mass until intersecting the persistent planes of the F1 and F7 joint sets or the topographic surface on the other side of the ridge are intersected. Table **5** shows the geometric characteristics of the volumes identified.

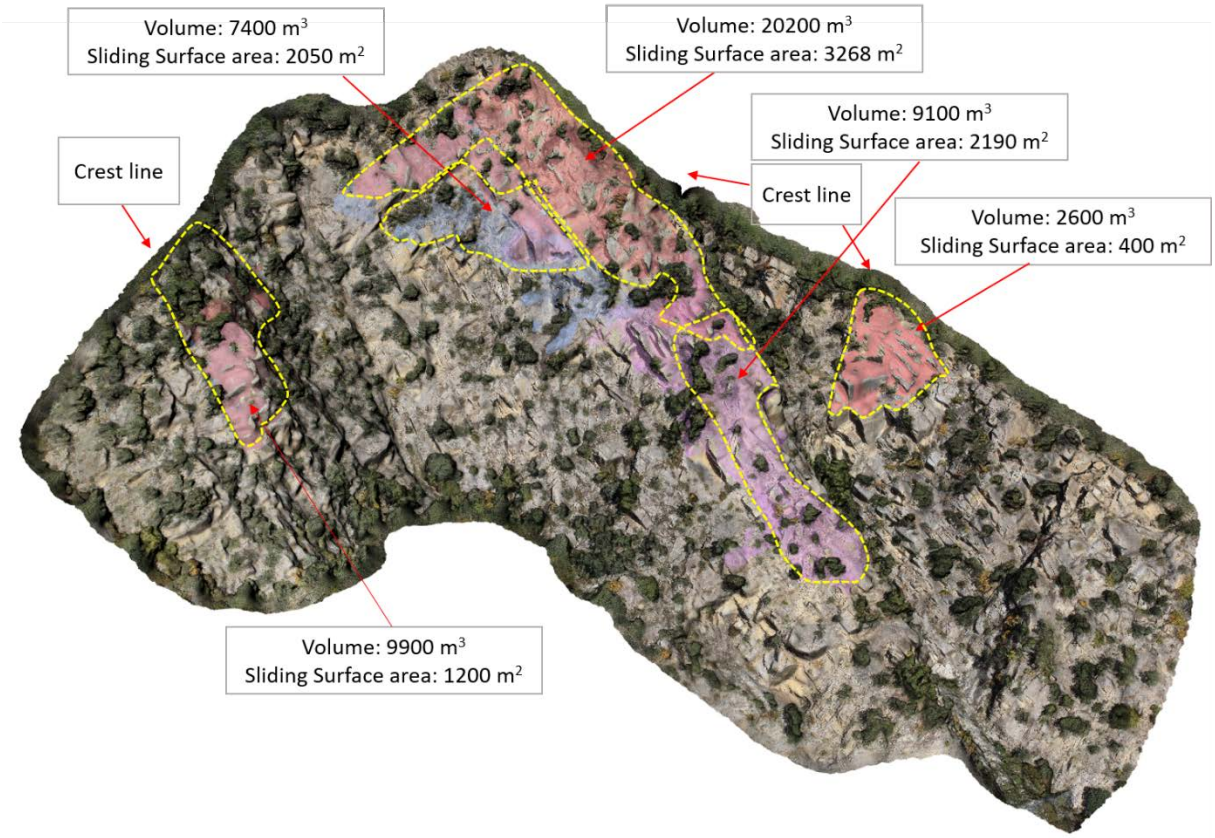

Figure 13. Texturized point cloud showing the largest volumes of rock spurs defined at the slope of Borrassica-Forat Negre

Roc spur	Basal plane area (F3 or F5 set) (m^2)	Volume of the rock mass (m^3)
BO-01	400	2600
BO-02	2190	9100
BO-03	3268	20200
BO-04	2050	7400
BO-05	1200	9900

Table 5. Volumes of the rock spurs identified at the slope of Borrassica – Forat Negre

We compared the volumes and basal areas of the rock spurs with the volumes estimated from the theoretical criteria of the Markland test used in the previous section. While the largest basal area identified from the Markland test is about 1300 m^2, the basal area of rock spurs is significantly bigger (up to 3270 m^2). However, the calculated volumes of the rock spurs are much smaller. This is due to the assumptions made in Mavrouli et al. (2015) on the persistence of the sliding planes and for converting areas to volumes. This supports the argument that the procedure used to calculate volumes with the simple kinematic approach overestimates the volume of potentially unstable rock masses and may set the highest bound for the MCE. Using this new approach (of 5volumes), the volumes that we obtain are lower than the 50,000 m^3 calculated previously.

The size distribution of scars obtained in equation [1] is the empirical evidence of rockfall events that have occurred in the past. However, the kinematically movable rock masses from individual rock spurs are scenarios that might occur in the future. Comparing the size of the largest volume calculated from the scars (approximately 3,000 m^3) and that of the most prominent rock spur (20,000 m^3) or of the rock wall under the criteria of the Markland test (50,000 m^3) is one order of magnitude. Although the difference is remarkable, it is worth noticing that none of the procedures used is capable to justify the volumes extrapolated from the F-M relation of Figure 2.

The areas of the basal planes under the rock spurs may reach up to > 3200 m^2. However, planes of this size are not observed in the basal plane of the scars, as the maximum surface measured for a basal plane of rupture is 213 m^2 (Mavrouli and Corominas, 2017), and cannot be justified either by fitting large planes to stepped down-dip adjacent planes.

An interesting detail of the area distribution of the planes measured with TLS (Figure **8**) is that a truncation of the power relationship (area - cumulative frequency) occur for both F3 and F5 joint sets, which causes a significant reduction of the number of planes over 100 area m^2 in relation to what is expected from the corresponding power law.

The truncation of the relationship is not fictitious as it applies to areas that have actually been identified and measured. Truncation may have a geological reason as it will be discussed in the next section. The truncation or deviation from the trend is also observed in other rockfall records, thus reducing the frequency of large rockfalls several orders of magnitude in relation to the previsions of the power law (Hungr et al. 1999; Guzzetti et al. 2003; Böhme et al. 2015).

5. Role of the geological structure

Lithology, structure and erosion history (i.e. glacial steepening and debutressing) are predisposing factors of rock slope failures (Evans and Clague, 1988). The role of the geologic structure for the generation of large rockslides and avalanches is well documented in the literature. The fracture pattern frequently facilitates the kinematic release of large slope failures (Guzzetti et al., 1996; Agliardi et al., 2001, 2009b; Badger, 2002; Massironi et al., 2003; Ambrosi and Crosta, 2006; Stead and Wolter, 2015). The sliding planes of large slope failures often develop along pre-existing planar features in the rock mass such as bedding planes, exfoliation joints, faults or cleavage dipping unfavourably towards de valley (Hermanns and Strecker, 1999; Keller, 2017) although in some regions this is not a requisite for the development large slope slope failures (Jarman, 2006; Cave and Ballantyne, 2016). On the contrary, the role of the geologic structure in constraining the size of the rock slope failures is less known.

In the Borrassica Forat Negre slope, Mavrouli and Corominas (2017) observed the frequent interruption of the basal planes (discontinuities F3 and F5) at their intersection with the tension crack and lateral release planes F7 and F1, respectively, which prevent the formation of large failures. Using independent procedures, they showed that the distribution of the exposed lengths along the dip of the F3 and F5 planes are similar to the distribution of the spacings of planes of F7. Furthermore, the analysis of the largest exposed lengths of F3 and F5 showed that, in some cases, a stepped sliding surface can be formed, which can be up to four times longer than the maximum spacing of F7. This fact suggested that in the Forat Negre slope, the failure surface may also generate by coalescence of several (although few) unfavourable dipping F3/F5 joints and/or by brittle failure of minor rock bridges. Some of these cases

were identified on photos (Figure 14). The maximum volume will therefore depend on the length of the basal plane and on the resistance of the rock bridges, if any.

Figure 14. Rockfall scar of April 20th, 2008. The failure developed over several adjacent down-dipping planes (F3) generating a stepped sliding surface (black solid line). Steps are formed F7 planes (yellow dashed polygons) and broken rock bridges. The failure is bounded laterally by planes of F1 set.

We performed a structural analysis of the joint sets of the Forat Negre looking for the reason of the interruption of the kinematically unstable joint sets that could justify the greater b-value of the scar volume distribution and a cutoff value for the largest expected volume. The field survey was carried out in the slopes of the granodiorite massif of Borrassica and Forat Negre, aiming at determining the relative chronology of the tectonic features affecting the rock mass (**Figure 15**). It was performed at key

outcrops where discontinuities are well exposed. The outcrops were studied by combining scanlines and detailed structural observations. It is found that set F6 was formed first as it is affected by other sets that interrupt and displace its planes. A second phase is characterized by sets F2 poorly identified with LiDAR and merged with F7. They should be interpreted as conjugate faults with F7. F3 is a joint set that could be associated to this phase. It shows high scattering and undulation with amplitude up to 20cm. The last phase is characterized by the occurrence of F1 and F4, which include both very persistent conjugate faults and joints that interrupt the rest of sets.

Fault sets (F1, F7) have a twofold role: they often interrupt and displace F3 and F5 joint sets; at the same time, they act as weak zones facilitating the formation of both the lateral and back release surfaces of the sliding rock masses.

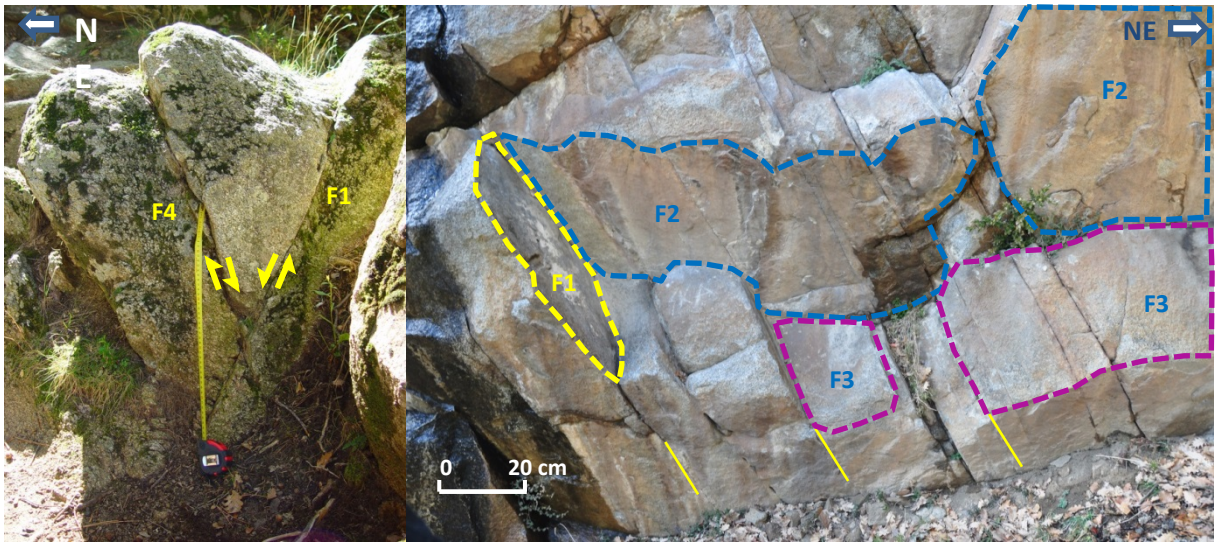

Figure 15. (left) Outcrop of conjugated faults F4 and F1; (right) intersection of planes of sets F1, F3 and F2 (from Corominas et al. 2017)

6. Discussion

We argue that we should not expect a random distribution of large landslides, in particular large rockslides and rock avalanches. In some regions there may exist a truncation for large volumes (upper size limit) and that geological factors may partially explain this behaviour.

7.1 Spatial distribution of large slope failures

Rock slope failures (RSF) is a term coined frequently found in geomorphological studies that encompasses three main slope instability forms (Ballantyne, 2002; Jarman, 2006; Cave and Ballantyne, 2016): catastrophic failures in the form rockslides, rock avalanches and major toppling; deep-seated gravitational slope deformations; complex failures involving two or more of the above. In the main mountain belts, RSF are often considered as paraglacial, implying that failure was preconditioned by the preceding episode of glaciation and deglaciation (Ballanyte, 2002; McColl, 2012). Despite a number of studies have focused on RSF, the knowledge of their distribution at a regional scale, timing and causes is still incomplete. The spatial analysis of the RSF suggests that a relation exists between the occurrence of the failures and the type of geological structures, the lithologies involved, and the inherited glacier relief/geomorphological setting (Jarman, 2006) or the triggers (Cave and Ballanyte, 2016; Crosta et al. 2016).

Regional inventories of large RSF have shown that:

a) RSF are uneven spatially distributed (Whalley et al 1983; Jarman 2006; Jarman et al. 2014; Strom 2015; Keller, 2017)
b) Greater density of occurrence on some susceptible lithologies (Cave and Ballantyne, 2016) but this is not a requisite in other locations (Strom, 2015)
c) Some events are recurrent in the same location (Shang et al. 2003; Hermanns et al. 2004; Evans et al. 2009; Delaney and Evans, 2015; Strom, 2015; Crosta et al. 2016)
d) Some regions are relatively rockslides-free areas (Strom, 2015).

Literature review shows that the density of landslides varies from one region to another and large rock slope failures are not evenly distributed in mountain regions. Jarman (2006) found in the Scottish Highlands that 65% of the large slope failures were concentrated in seven main clusters while the rest were non-randomly scattered. In Iceland, large rockslides occur almost entirely on (within) a particular lithological unit (Tertiary lavas), particularly in locations where the lava layers dip towards the valley (Whalley et al. 1983).

The first comprehensive study of large-scale rock slope failures in the Eastern Pyrenees where the Solà d'Andorra is located, identified 30 main large slope failures and further 20 smaller or uncertain cases (Jarman et al. 2014). The inventory did not show any obvious regional pattern or clustering and a surprisingly sparse population that affects 45–60 km^2 or 1.5–2.0% of the 3000 km^2 glaciated core of the mountain range and neighbouring fluvial valleys. From them, only 27% can be considered as large

668 catastrophic events (rock or debris avalanches) and none of them were located in the Valira river valley.
669 For comparison, in the Alps, 5.6% of the entire 6200 km^2 montane area is affected by deep-seated
670 gravitational slope deformations alone (Crosta et al. 2013) and up to 11% in the Upper Rhone basin
671 (Pedrazzini et al (2016). This sparsity has been interpreted by a low-intensity glaciation and less
672 subsequent debuttressing, relative tectonic stability and small fluvial incision (Jarman et al. 2014). When
673 compared to other mountain ranges, the Pyrenees have been less steepened and incised by the
674 Pleistocene glaciers. The slopes in the Valira valleys commonly rise 1000m from valley bottoms,
675 reaching a maximum of up to1400m. In the Karakoram, the Southern Alps of New Zealand and in the
676 Pacific Coastal Ranges of USA and Canada, the slopes usually rise 3000m and some may attain more
677 than 6000m (Hewitt et al. 2008).
678
679 ***7.2 Truncation of the power laws***
680
681 Many natural processes are described by power law distributions such as fault displacements (Kakimi,
682 1980), fault trace length (Bonnet el al 2001), earthquakes (Gutenberg and Richter, 1954). Data collected
683 to measure the parameters of such distributions only represents samples from some underlying
684 population. Without proper consideration of the scale and size limitations of such data, estimates of the
685 population parameters, particularly the exponent of the power law, are likely to be biased (Pickering et
686 al. 1995). As stated by Hovius et al. 1997, extrapolating short-term geomorphic observation to time
687 scales pertinent to landscape development requires an understanding of the scaling behaviour of the
688 processes involved, in particular the magnitude and frequency with which they occur (Wolman and
689 Miller, 1960; Hovius et al. 1997). All power law and fractal characteristics in nature must have upper
690 and lower bounds (Bonnet el al. 2001).
691
692 All the evidences suggest that an upper limit to the size of the slope failures in the Sola d'Andorra might
693 exist. These observations are consistent with the findings of Hergarten (2012), who applied a simple
694 model for rock detachment in the Alps, Southern Rocky Mountains and the Himalayas. He found a
695 breakdown of the power law distributions at large events. Large slope failures occur less frequently than
696 predicted by the power laws and the size at which the cut-off takes place, varies from one region to
697 other. Furthermore, the size of largest event at each region may differ more than one order of magnitude.
698 These differences were attributed to the different geologic and climatic contexts although a detailed
699 work was not carried out. Clarke and Burbank (2010) compared the occurrence of rock slope failures in
700 Fiorland and western Southern Alps in New Zealand. These two regions are subjected to similar climate
701 but different uplift rates and lithologies. They observed that despite failures initiate on slopes steeper

than the modal hillslope angle in both regions, the frequency-magnitude distributions revealed one order of magnitude difference, being considerably smaller and less frequent in Fiorland. These authors conclude based on geophysical surveys that the dense geomorphic fracturing in Fiorland appears to limit the depth and magnitude of the slope failures. Conversely, in the Southern Alps, fractures are more pervasive and result in larger and deeper landslides.

The incompleteness of the record or the use of different criteria for fitting of the power laws to the volume distributions may therefore produce significant differences in the estimation of the frequency of large events.

7.3 Role of the geological factors

The assumption of spatial random distribution of the slope failures overlooks the basic geomechanical prerequisites (rock strength, fracture pattern, relief,..) for failure (Selby, 1992; Jarman, 2006) as it is evident that some geological contexts (i.e. steeply dipping discontinuities or weak lithologies) favour the occurrence of the slope failures. Tectonic damage has also been accounted for several stepped large rock slope failures (Brideau et al 2009). In our work, we argue that the fracture pattern (geological context) of the Solà d'Andorra plays a key role in constraining the size (defining the cutoff size) of large rockslope failures. Fault sets (F1, F7) have a twofold role: they interrupt the continuity of the planes of the F3 and F5 joint sets; at the same time, they act as weak zones facilitating the formation of both the lateral and back release surfaces of the sliding rock masses.

It is also evident that other factors can be accounted for. In alpine mountain glacial and fluvial incision of the valley bottoms causes steepening of the valley slopes that induces slope failures (Selby, 1980). In tectonically active regions, the sustained rock uplift and valley incision perpetuates this process and results in a landslide-dominated landscape (denudation) (Burbank, et al. 1996). The analysis of the slope angles distribution in tectonically active mountain belts has shown that there exists threshold conditions of slope inclination or height at which they fail readily because of limitations in material strength (Korup et al. 2007).

Therefore, the scarce number of large rock slope failures and rock avalanche deposits in Andorra should not be considered an exception. Low density of RSF has been also observed in Scotland (Cave and Ballantyne, 2016)

7. Conclusions

This paper through the analysis of the rockfall occurrence at the rock wall of Borrassica-Forat Negre of the Solà d'Andorra addresses the validity of the extrapolation of the M-F relations obtained far beyond the temporal window used for their preparation. We argue that despite the M-F relation is well fitted, there exist no evidences supporting the occurrence of large slope failures (larger than 100,000m^3) in the Solà d'Andorra at least, during the last 10,000 years. Neither rockslide/rock avalanche deposits were found in the Valira river valley bottom nor evident large detachment scars (rockfall cavities) are identified in the rock walls from the analysis of the TLS-generated point cloud of the outcropping surfaces.

According to the geo-structural analysis (fracture pattern) and the geomorphological evidences, the most predominant slope failure mechanism is planar sliding. The largest continuous exposed sliding surface has an area of 200 m^2 while the M-F relation of the surfaces measured is truncated at around 50m^2. The volume distribution of 5000 rockfall scars generated stochastically by combining the measured areas of the basal sliding surfaces and the scar heights, which may cover a time span of several thousands of years, yielded a maximum rockfall scar volume of 3000 m^3 (Santana et al. 2012). No evidences have been found that could justify the occurrence of a large stepped failure in the past.

Two independent procedures have been applied to measure the size of the kinematically detachable rockfall masses according to Markland instability criteria (Mavrouli and Corominas 2017) and the size of rock spurs lying over unfavourable dipping joints that have been assumed as highly persistent. The largest volumes identified are of a few tens of thousands of cubic meters only. These results are consistent with the absence of rock slide or rock avalanche deposits at the bottom of the Andorra la Vella basin.

The detachment of large rock masses via a continuous surface is prevented by the geological structure. The interruption of the sliding planes by two orthogonal highly persistent sets of faults (F1 and F7), restrict the development of large rock mass volumes. The volume restriction can be overcome to some extent either by coalescence of basal planes or through step-path failures involving the breakage of rock bridges. This situation however, will necessarily involve smaller volumes than in the case of fully persistent basal joints. Because of this, we conclude that the maximum credible volume for Forat Negre is significantly smaller than the expected from the basic kinematical analysis of the rock slope. The latter

was estimated between 25,000 and 50,000 m^3 (Mavrouli et al .2017). The case of Andorra provides empirical evidence that rockfall could be size-constrained due to the geological structure.

The lack of large slope failures in this reach of the Valira river valley should not be considered as an anomaly because several studies in mountainous ranges worldwide have demonstrated that large rockslides and rock avalanches are not randomly distributed in the space and that local geological and geomorphic conditions exert some control on the development of the slope failures.

Based on all these considerations, we conclude that the M-F relations should not be exported from one region to another without taking into account the particular characteristics of the involved slopes.

Acknowledgments

This work has been carried out with the support of the fellowship to the third author and within the framework of the research project Rockmodels financed by the Spanish Ministry of Economy and Competitiveness (BIA2016-75668-P) and by the Government of Andorra (Edicte de 10/04/2013, BOPA nº18 17/04/2014). We thanks the Parc Nacional d'Aigüestortes i Estany de Sant Maurici for the support provided for the survey with TLS at Pala Morrano slope.

References

Abbruzzese JM, Sauthier C, Labiouse V (2009) Considerations on Swiss methodologies for rock fall hazard mapping based on trajectory modelling. Nat Hazards Earth Syst Sci 9:1095-1109

Agliardi F, Crosta G, Zanchi A (2001) Structural constraints on deep-seated slope deformation kinematics. Engineering Geology 59: 83–102.

Agliardi F, Crosta GB, Frattini P (2009a) Integrating rockfall risk assessment and countermeasure design by 3D modelling techniques. Nat Hazards Earth Syst Sci, 9: 1059-1073

Agliardi F, Crosta GB, Zanchi A, Ravazzi C (2009b) Onset and timing of deep-seated gravitational slope deformations in the eastern Alps, Italy. Geomorphology 103: 113–129.

Ambrosi C, Crosta GB (2006) Large sackung along major tectonic features in the Central Italian Alps. Engineering Geology 83: 183–200

Amigó J, Altimir J, Copons R (2001) Verificación de los resultados del modelo de simulación Eurobloc a partir de casos reales de caídas de bloques rocosos. V Simposio Nacional sobre Taludes y Laderas Inestables. Madrid. Vol. 2: 653-663.

Badger TC (2002) Fracturing within anticlines and its kinematic control on slope stability.

802 Environmental and Engineering Geoscience VIII: 19–33.
803 Ballantyne CK (2002) Paraglacial geomorphology. Quaternary Science Reviews 21: 1935-2017
804 Ballantyne CK, Stone JO (2004) The Beinn Alligin rock avalanche, NW Scotland: Cosmogenic 10Be
805 dating, interpretation and significance. The Holocene 14: 448-453
806 Barlow J, Lim M, Rosser N, Petley D, Brain M, Norman E, Geer M (2012) Modeling cliff erosion using
807 negative power law scaling of rockfalls.Geomorphology 139: 416-424
808 Barton N, Bandis S (1982) Effects of block size on the shear behavior of jointed rock. The 23rd U.S
809 Symposium on Rock Mechanics, Berkeley, California. pp. 739-760
810 Böhme M, Oppikofer T, Jaboyedoff M, Hermanns RJ, Derron MH (2015) Analyses of past and present
811 rock slope instabilities in a fjord valley: Implications for hazard estimations. Geomorphology 248:
812 464–474
813 Bonnet E, Bour O, Odling NE, Davy P, Main I, Cowie P, Berkowitz B (2001) Scaling of fracture systems
814 in geological media. Reviews in Geophysics, 39: 347-383
815 Bourrier F, Dorren L, Hungr O (2013) The use of ballistic trajectory and granular flow models in
816 predicting rockfall propagation. Earth Surf Processes Landforms 38: 435–440
817 Brardinon, F, Church M (2004) Representing the landslide magnitude–frequency relation: Capilano
818 River Basin, British Columbia. Earth Surface Processes and Landforms 29: 115–124
819 Brideau MA, Yan M, Stead D (2009) The role of tectonic damage and brittle rock fracture in the
820 development of large rock slope failures. Geomorphology 103: 30-49
821 Brundl M, Romang HE, Bischof N, Rheinberger CM (2009) The risk concept and its application in
822 natural hazard risk management in Switzerland. Nat. Hazards Earth Syst. Sci., 9: 801–813
823 Burbank DW, Leland J, Fielding E, Anderson RS, Brozovic RS, Reid MR, Duncan C (1996) Bedrock
824 incision, rock uplift and threshold hillslopes in the northwestern Himalayas. Nature, 379: 505-510
825 Cascini L, Bonnard C, Corominas J, Jibson R, Montero-Olarte J 2005. Landslide hazard and risk zoning
826 for urban planning and development. State of the art report (SOA7). In: Hungr O, Fell R, Couture
827 R, Eberthardt E (eds) Proceedings of the international conference on “landslide risk management”,
828 Vancouver (Canada). Taylor and Francis, London, pp 199–235
829 Cave JAS, Ballantyne CK (2016) Catastrophic Rock-Slope Failures in NW Scotland: Quantitative
830 Analysis and Implications. Scottish Geographical Journal 132: 185-209
831 Chau KT, Wong RCH, Liu J, Lee CF (2003) Rockfall Hazard Analysis for Hong Kong Based on
832 Rockfall Inventory. Rock Mech Rock Eng 36: 383–408
833 Clarke BA, Burbank DW (2010) Bedrock fracturing, threshold hillslopes and limit to the magnitude of
834 landslides. Earth and Planetary Science Letters 297: 577-586

835 Copons, R, Altimir J, Amigó J, Vilaplana JM (2001) Medotología *Eurobloc* para el estudio y protección
836 de caídas de bloques rocosos. Principado de Andorra. V Simposio Nacional sobre Taludes y
837 Laderas Inestables. Madrid. Vol. 2: 665-676.
838 Copons R, Vilaplana JM, Corominas J, Altimir J, Amigó J (2004) Rockfall risk management in high-
839 density urban areas. The Andorran experience. In: T.Glade, M. Anderson and M.J. Crozier (eds).
840 Landslide hazard and risk. John Wiley and Sons, Chichester. pp. 675-698.
841 Copons R (2007) Avaluació de la perillositat de caigudes de blocs rocosos al Solà d'Andorra la Vella.
842 Monografies del CENMA
843 Corominas, J. (1996) The angle of reach as a mobility index for small and large landslides, Canadian
844 Geotechnical Journal, 33: 260–271.
845 Corominas J, Copons R, Vilaplana JM, Altimir J, Amigó, J (2003) Integrated landslide susceptibility
846 analysis and hazard assessment in the principality of Andorra. Nat Hazards, 30: 421–435
847 Corominas J (2007) Experience on landslide risk management in the Eastern Pyrenees (Spain and
848 Andorra): achievements and challenges. In K. Ho and V. Li (Eds). The 2007 International Forum on
849 Landslide Disaster Management. Hong Kong. The Hong Kong Institution of Engineers. Vol 1: 49-70
850 Corominas J, Copons R, Moya J, Vilaplana, J M, Altimir J, Amigó J (2005) Quantitative assessment of
851 the residual risk in a rock fall protected area. Landslides 2: 343–357
852 Corominas J, Moya J (2008) A review of assessing landslide frequency for hazard zoning purposes. Eng
853 Geol 102: 193-213
854 Corominas J, van Westen C, Frattini P, Cascini L, Malet JP, Fotopoulou S, Catani F, Van Den Eeckhaut
855 M, Mavrouli O, Agliardi F, Pitilakis K, Winter MG, Pastor M, Ferlisi S, Tofani V. Hervás J, Smith
856 JT (2014) Recommendations for the quantitative analysis of landslide risk. Bull Eng Geol Env 73:
857 209-263.
858 Crosta GB, Frattini P, Agliardi F (2013) Deep seated gravitational slope deformations in the European
859 Alps. Tectonophysics 605: 13–33.
860 Crosta GB, Hermanns RL, Dehls J, Lari S, Sepulveda S (2016) Rock avalanches clusters along the
861 northern Chile coastal scarp, Geomorphology, doi:10.1016/j.geomorph.2016.11.024
862 Cruden D M (1975) Major rock slides in the Rockies. Canadian Geotechnical Journal 13, 8–20.
863 Cruden DM (1985) Rock slope movements in the Canadian Cordillera. Canadian Geotechnical Journal
864 22: 528–540.
865 Cruden DM Varnes DJ (1996) Landslide types and processes. In, Landslides Investigation and
866 Mitigation, A. K. Turner and R. L. Schuster, eds.: National Research Council, Transportation
867 Research Board, Special Report 247: 36-75
868 Cruden DM, Hu XQ (1993) Exhausting and steady state models for predicting landslide hazards in the

869 Canadian Rocky Mountains. Geomorphology 8: 279-285
870 Davies TR, McSaveney MJ (2002) Dynamic simulation of the motion of fragmenting rock avalanches.
871 Canadian Geotechical Journal 39:789–798
872 Delaney KB Evans SG (2015) The 2000 Yigong landslide (Tibetian Plateau), rockslide- dammed lake
873 and outburst flood: review, remote sensing analysis and process modeling. Geomorphology 246:
874 377-393
875 Dussauge-Peisser A, Helmstetter A, Grasso, JR, Hanz D, Desvarreux P, Jeannin M, Giraud A. (2002)
876 Probabilistic approach to rockfall hazard assessment: potential of historical data analysis. Nat
877 Hazards Earth Syst Sci 2: 15-26.
878 Dussauge C, Grasso JR, Helmstetter A (2003) Statistical analysis of rockfall volume distributions:
879 Implications for rockfall dynamics. J Geophys Res B6 108: 2286
880 Eberhardt E, Stead D, Coggan JS (2004) Numerical analysis of initiation and progressive failure in
881 natural rock slopes - the 1991 Randa rockslide. Int. J. Rock Mech. Mining Sciences 41: 69-87.
882 Escalé J (2001) La nova llei d'ordenament territorial a Andorra. In La Gestió dels Riscos naturals.
883 Primeres Jornades CRECIT. Andorra la Vella. http://www.iea.ad/crecit/primeresjornades.html.
884 Evans SG, Clague JJ (1988) Catastrophic rock avalanches in glacial environments. In: Bonnard, C. (Ed.),
885 5th International Symposium on Landslides, Lausanne, Switzerland, 2, pp. 1153–1158.
886 Evans S, Hungr O (1993) The assessment of rockfall hazard at the base of talus slopes. Canadian
887 Geotechnical Journal 30: 620-636
888 Evans SG, Bishop NF, Smoll LF, Murillo PV, Delaney KB, Oliver-Smith A (2009) A reexamination
889 of the mechanism and human impact of catastrophic mass flows originating on Nevado Huascarán,
890 Cordillera Blanca, Peru, in 1962 and 1970. Engineering Geology 108: 96-118.
891 Fell R, Corominas J, Bonnard Ch, Cascini L, Leroi E, Savage WZ (on behalf of the JTC-1 Joint
892 Technical Committee on Landslides and Engineered Slopes) (2008) Guidelines for landslide
893 susceptibility, hazard and risk zoning for land use planning. Eng. Geology 102: 85–98
894 Ganerød GV, Grøneng G, Rønning JS, Dalsegg E, Elvebakk H, Tønnesen JF, Kveldsvik V, Eiken T,
895 Blikra LH, Braathen A (2008) Geological model of the Åknes rockslide, western Norway.
896 Engineering Geology, 102: 1-18.
897 Gigli G, Frodella W, Garfagnoli F, Morelli S, Mugnai F, Menna F, Casagli N (2014) 3-D geomechanical
898 rock mass characterization for the evaluation of rockslide susceptibility scenarios. Landslides 11:
899 131-140.
900 Guthrie R, Evans SG (2004) Analysis of landslide frequencies and characteristics in a natural system.
901 Coastal British Columbia. Earth Surface Processes and Landforms 29, 1321–1339
902 Gutiérrez-Rodríguez MC, Turu V (2013) Hidrogeología de un valle glaciar: el caso de la cubeta de

903 Andorra (Pririneos Orientales). Parte 1: datos geoquímicos. X Simposio de Hidrogeología.
904 Granada.
905 http://www.igeotest.ad/igeofundacio/Activitats/Docs/PDF/Granada/articulo%20hidro%206_Parte
906 %201e.pdf
907 Guttemberg B, Richter CF (1954) Seismicity of Earth and associated phenomena (2nd Ed.) Princeton
908 University Press, Princeton, NJ.
909 Guzzetti F, Cardinali M, Reichenbach P (1996) The influence of structural setting and lithology on
910 landslide type and pattern. Environmental and Engineering Geosciences 2: 531–555.
911 Guzzetti F, Malamud BD, Turcotte DL, Reichenbach P (2002) Power-law correlations of landslide areas
912 in Central Italy. Earth Planet Sci Lett 195: 169-183
913 Guzzetti F, Reichenbach P, Wieczorek GF (2003) Rockfall hazard and risk assessment in the Yosemite
914 Valley, California, USA. Nat Hazards Earth Syst Sci 3: 491–503.
915 Guzzetti, F., F. Ardizzone, M. Cardinali, M. Rossi, and D. Valigi (2009), Landslide volumes and
916 landslide mobilization rates in Umbria, central Italy, Earth Planet. Sci. Lett., 279, 222–229
917 Hergarten S (2012) Topography-based modeling of large rockfalls and application to hazard assessment,
918 Geophys. Res. Lett. 39, L13402, doi:10.1029/2012GL052090.
919 Hermanns RL, Strecker MR (1999) Structural and lithological controls on large Quaternay rock
920 avalanches (sturzstroms) in arid northwestern Argentina. Geological Society of America Bulletin,
921 111: 934-948
922 Hermanns RL, Niedermann S, Ivy-Ochs S, Kubik PW (2004) Rock avalanching into a landslide dammed
923 lake causing multiple dam failure in Las Conchas valley (NW Argentina) - evidence from surface
924 exposure dating and stratigraphic analyses. Landslides 1: 113 - 122.
925 Hewitt K, Clague JJ, Orwin JF (2008) Legacies of catastrophic rock slope failures in mountain
926 landscapes. Earth-Sci Reviews, 87: 1–38
927 Ho KKS (2004) Recent advances in geotechnology for slope stabilization and landslide mitigation –
928 perpective from Hong Kong. In: Lacerda, W.A., Ehrlich, M., Fontoura S.A.B., Sayao, A.S.F (eds)
929 Landslides: Evaluation and Stabilization.. Taylor and Francis, London, UK. Vol. 2 pp. 1507-1560
930 Hsü KJ (1978) Albert Heim: observations of landslides and relevance to modern interpretations. In:
931 Voight, B. (Ed.), Rockslides and Avalanches; 1, Natural Phenomena. Elsevier, Amsterdam, pp. 70–
932 93.
933 Hovius N, Stark CP, Allen PA (1997) Supply and removal of sediment in a landslide-dominated
934 mountain belt: Central Range, Taiwan. Journal of Geology 108: 73-89
935 Hungr O, Evans SG, Hazzard J (1999) Magnitude and frequency of rock falls and rock slides along the
936 main transportation corridors of southwestern British Columbia. Canadian Geotechnical Journal,

36: 224-238

Hungr O, Leroueil S, Picarelli L (2014) The Varnes classification of landslides types, an update. Landslides 11:167-194.

Jarman D (2006) Large rock slope failures in the Highlands of Scotland: characterisation, causes and spatial distribution. Engineering Geology, 83: 161-182

Jarman D, Calvet M, Corominas J, Delmas M, Gunnell Y (2014) Large-Scale Rock Slope Failures in the Eastern Pyrenees: Identifying a Sparse But Significant Population in Paraglacial and Parafluvial Contexts. Geogr Ann A 96 (3): 357-391.

Kakimi T (1980) Magnitude frequency relation for displacement of minor faults and its significance in crustal deformation. Bull. Geol. Society of Japan, 31: 467-487

Keller B (2017) Massive rock slope failure in Central Switzerland: history, geologic–geomorphological predisposition, types and triggers, and resulting risks. Landslides DOI 10.1007/s10346-017-0803-1

Klar A., Aharonov E., Kalderon-Asael B., Katz O., 2011. Analytical and observational relations between landslide volume and surface area, Journal of Geophysical Research, vol. 116, 1–10

Korup O, Clague JJ, Hermanns RL, Hewitt K, Strom AL Weidinger JT (2007) Giant landslides, topography and Erosion, Earth and Planetary Science Letters 261: 578–589

Lari S, Frattini P, Crosta GB (2014) A probabilistic approach for landslide hazard analysis. Engineering Geology 182: 3-14

Li ZH, Huang HW, Xue YD, Yin J (2009) Risk assessment of rockfall hazards on highways. Georisk, 3: 147-154

Malamud BD, Turcotte DL, Guzzetti F (2004) Landslide inventories and their statistical properties. Earth Surface Processes and Landforms 29: 687–711

Marques FMSF (2008) Magnitude-frequency of sea cliff instabilities. Nat. Hazards Earth Syst. Sci. 8: 1161–1171,

Massironi M, Bistacchi A, Dal Piaz GV, Monopoli B, Schiavo A (2003) Structural control on mass-movement evolution: a case study from the Vizza Valley, Italian Eastern Alps. Eclogae Geologicae Helvetiae 96: 85–98.

Mavrouli O, Corominas J, Jaboyedoff M (2015) Size distribution for potentially unstable rock masses and in-situ rock blocks using LIDAR generated Digital Elevation Models. Rock Mechanics Rock Engineering 48: 1589-1604

Mavrouli O, Corominas J (2017) Comparing rockfall scar volumes and kinematically detachable rock masses. Engineering Geology, 219: 64–73

McColl ST (2012) Paraglacial rock-slope stability. Geomorphology, 153-154: 1-16

971 Pedrazzini A, Humair F, Jaboyedoff M, Tonini M (2016) Characterisation and spatial distributionof
972 gravitational slope deformation in the Upper Rhone catchment (Western Swiss Alps). Landslides
973 13: 259–277
974 Picarelli L, Oboni F, Evans SG, Mostyn G, Fell R (2005) Hazard characterization and quantification. In
975 O. Hungr, R. Fell, R. Couture and E. Eberthardt (editors) Landslide Risk Management. Taylor and
976 Francis, London. pp. 27-61 ISBN: 041538043X
977 Pickering G., Bull, JM, Sanderson DJ (1995) Sampling power-law distributions. Tectonophysics, 248:
978 1-20
979 Rochet L (1987) Application des modeles numeriques de propagation a l'etude des eboulements
980 rocheux. Bull Lab Ponts et Chaussées 150/151: 84–95
981 Rosser N, Lim M, Petley D, Dumming S, Allison R (2007) Patterns of precursory rockfall prior to slope
982 failure. J Geophys Res 112: F04014,
983 Rossi M, Witt A, Guzzetti F, Malamud B D, Peruccacci S (2010) Analysis of historical landslide time
984 series in the Emilia-Romagna region, northern Italy. Earth Surface Processes and Landforms 35:
985 1123-1137
986 Royán MJ, Abellán A, Jaboyedoff M, Vilaplana JM, Calvet J (2014) Spatio-temporal analysis of rockfall
987 pre-failure deformation using Terrestrial LiDAR. Landslides 11: 697–709.
988 Royán M J, Abellán A, Vilaplana JM. (2015) Progressive failure leading to the 3 December 2013
989 rockfall at Puigcercós scarp (Catalonia, Spain). Landslides 12: 585–595
990 Santana D, Corominas J, Mavrouli O, Garcia-Selles D (2012) Magnitude-Frequency relation for
991 rockfalls using a Terrestrial Laser Scanner. Engineering Geology 145–146: 50-64
992 Scheidegger AE (1973) On the prediction of reach and velocity of catastrophic landslides. Rock
993 Mechanics 5: 231–236.
994 Selby MJ (1980) A Rock mass strength classification ofr geomorphic processes: with tests from
995 Antartica and New Zealand. Zeits. Fur Geomorphologie 24: 31-51
996 Selby MJ (1992) Hillslope Materials and Processes. University Press, Oxford.
997 Shang Y, Yang Z, Li L, Liu D,Liao Q, Wang Y (2003) A super-large landslide in Tibet in 2000:
998 background, occurrence, disaster, and origin. Geomorphology 54: 225 - 243
999 Soeters R, Van Westen C J (1996) Slope instability, recognition, analysis and zonation. In: Turner, AT,
1000 Schuster, RL (ed), Landslides — Investigation and Mitigation, Transportation Research Board
1001 Special Report No 247 National Academy Press, Washington DC, pp 129-177
1002 Stark CP, Hovius N (2001) The characterization of the landslide size distributions. Geoph. Res Letters,
1003 28: 1091-1094
1004 Stead, D, Wolter A (2015) A critical review of rock slope failure mechanisms: The importance of

structural geology. Journal of Structural Geology, 74: 1-23

Strom A (2015) Clustering of large bedrock landslides and recurrent slope failure: implications for lands seismic hazard assessment of the Tien Shan – Djungaria region. International Journal of Geohazards and Environment, 1: 110-121

Sturzenegger M, Stead D (2012) The Palliser Rockslide, Canadian Rocky Mountains: Characterization and modeling of a stepped failure surface. Geomorphology 138: 145–161

Swain RE, England JF Jr, Bullard KL, Raff DA (2006) Guidelines for evaluating hydrologic hazards, U.S. Department of Interior, Bureau of Reclamation, Denver, CO, 83 p.

Turner AK, Jayaprakash GP (2012) Introduction. In A.K. Turner & R.L. Schuster (Eds). Rockfall characterization and control. Transportation Research Board, National Academy of Sciences. Whasington D.C. pp. 3-20

Turu V, Boulton,G, Ros X, Peña, JL, Martí C, Bordonau J, Serrano E, Sancho C, Constante A, Pous J, González JJ, Palomar J, Herrero R, García JM (2007) Structure des grands bassins glaciaires dans le nord de la Péninsule Ibérique: comparaison entre les vallées d'Andorre (Pyerénées orientales), du Gállego (Pyrénées centrales) et du Trueba (Chaîne Cantabrique); Quaternaire, vol. 18/4, 309-325 http://quaternaire.revues.org/index1167.html

Turu V, Calvet M, Bordonau J, Gunnell Y, Delmas M, Vilaplana JM, Jalut G (2016) Did Pyrenean glaciers dance to the beat of global climatic events? Evidence from the Würmian sequence stratigraphy of an ice-dammed paleolake depocentre in Andorra. In: Quaternary Glaciation in the Mediterranean Region. Geological Society, Special Publication. London. 433.

UN/ISDR (2004) Living with Risk: A Global Review of Disaster Reduction Initiative, United Nations Publication, Geneva.

USBR (2015) Best practices in dam and levee safety risk analysis. Version 4.0 USBR, USACE. https://www.usbr.gov/ssle/damsafety/risk/BestPractices

Voight B, Pariseau WG (1978) Rockslides and avalanches: an introduction. In: Voight, B. (Ed.), Rockslides and Avalanches, 1 Natural Phenomena. Elsevier, NY, pp. 1–67.

Wang X, Frattini P, Crosta G, Zhang L, Agliardi F, Lari S, Yang Z (2014) Uncertainty assessment in quantitative rockfall risk assessment. Landslides 11:711–722

Whalley WB, Douglas GR, Jonsson A (1983) The magnitude and frequency of large rockslides in Iceland in the postglacial. Geografiska Annaler 65A: 99-110

Willenberg H, Löw S, Eberhardt E, Evans KF, Spillman T. Heinke B, Maurer H, Green AG (2008.) Internal structure and deformation of an unstable crystalline rock mass above Randa (Switzerland): part I e internal structure from integrated geological and geophysical investigations. Eng. Geology, 101: 1-14.

1039 Wolman MG, Miller JP (1960) Magnitude and frequency of forces in geomorphic processes. Journal of
1040 Geology 68: 54–74.
1041 Wolter A, Stead D, Clague JJ (2014) A morphologic characterisation of the 1963 Vajont Slide, Italy,
1042 using long-range terrestrial photogrammetry. Geomorphology 206 : 147-164
1043